IEEE Access
Multidisciplinary | Rapid Review | Open Access Journal

Received June 16, 2020, accepted July 5, 2020, date of publication July 15, 2020, date of current version July 24, 2020.

Digital Object Identifier 10.1109/ACCESS.2020.3009367

Analysis of High Impedance Coils Both in Transmission and Reception Regimes

MASOUD SHARIFIAN MAZRAEH MOLLAEI[1], CAREL C. VAN LEEUWEN[2], ALEXANDER J. E. RAAIJMAKERS[2], AND CONSTANTIN R. SIMOVSKI[1]

[1]Department of Electronics and Nanoengineering, Aalto University, 02150 Espoo, Finland
[2]Department of Radiology, UMC Utrecht, 3584 Utrecht, The Netherlands

Corresponding author: Masoud Sharifian Mazraeh Mollaei (masoud.2.sharifianmazraehmollaei@aalto.fi)

This work was supported by the European Union's Horizon 2020 Research and Innovation Program under Grant 736937.

ABSTRACT Theory of a high impedance coil (HIC) – a cable loop antenna with a modified shield – is comprehensively discussed for MRI application in both transmitting and receiving regimes. Understanding a weakness of the previously reported HIC in transmitting regime, we suggest another HIC which is advantageous in both transmitting and receiving regimes compared to a conventional loop antenna. In contrast with the claim of previous works that the reported HICs are advantageous in transmission regime, we show only this HIC is a practical transceiver HIC. Using the perturbation approach and adding gaps to both shield and inner wire of the cable, we tune the resonance frequency to be suitable for ultra-high field (UHF) magnetic resonance imaging (MRI). These gaps reduce the quality factor of the enhanced HIC which makes its resonant frequency more stable with respect to different loadings. Our theoretical model and applicability of our HIC for MRI applications are verified by simulations. Using the theoretical model, we have designed and fabricated an array of three HICs operating at 298 MHz. The operation of the array has been experimentally studied in the presence of different phantoms used in ultrahigh field MRI and the results compared with those obtained for a conventional array.

INDEX TERMS High impedance, magnetic resonance imaging, transceiver antenna.

I. INTRODUCTION

Phased array antennas play a key role in modern magnetic resonance imaging (MRI) to increase spatial resolution and efficiency compared to conventional radio-frequency coils. Since in these phased arrays, the elemental antennas are tightly packed, their coupling becomes a critical issue. In transmitting regime, this coupling results in cross-talks, inter-channel scattering and lower efficiency. In receiving regime, it results in increased noise correlation which decreases the efficiency [1]–[5].

For scanning specific parts of a human body such as the head, arrays of loop antennas are used. In many MRI schemes, the methods of decoupling the loop antennas imply their partial overlapping. In this way one can cancel out the mutual inductance between adjacent loops. However, in arrays with many loop antennas in a cylindrical configuration applied in ultra-high field (UHF) MRI, these techniques are sometimes not sufficient. In fact, due to rather high operating frequency in UHF MRI, the coupling of loops is not purely inductive and non-neighbouring loops remain noticeably coupled [3], [6].

Recently, a novel approach for decoupling of loop antennas was suggested which uses the property of a Huygens element to create a null of the electromagnetic field in the near zone [7]. In this coils, a lumped capacitor is located at a top point of the loop (which is opposite to the feeding point). When this capacitance is sufficiently small, the current distribution in the coil is not uniform – besides of a magnetic dipole mode (uniform current) an electric dipole mode (in-phase with the magnetic dipole mode current on the top of coil and opposite-phase on the bottom) are excited. Properly choosing the value of this capacitance, magnetic coupling coefficient and electric coupling coefficient become balanced and opposite in phase. This grants the decoupling for two adjacent loops having nulls of their near-field pattern on the line connecting their centers. However, the coupling of non-neighboring antennas keeps noticeable. Moreover, this technique is not convenient for scanning the movable organs as hand and knee [8].

Using concept of non-radiative coil in wireless power transfer [9], [10], a new type of coils with high input impedance called high impedance coil (HIC) was suggested

The associate editor coordinating the review of this manuscript and approving it for publication was Haiwen Liu.

in [8] (similar works can be seen in [11]–[15]). This HIC is introduced as a receiving loop antenna made of a coaxial cable with a gap in the shield on the top of the loop (opposite side of the receiver location) and the central conductor is connected to the receiver through a hole in the shield on the bottom of the loop. The high impedance does not allow the induced current to flow that results in the absence of scattering. This antenna was designed for a high-field MRI (operating frequency 123 MHz). In this paper, we aim to modify this receiving antenna qualitatively so that to make it suitable for UHF MRI. Here not only the operation frequency is much higher but also the antenna should operate in the transceiver regime.

The possibility of a HIC to operate in the transmission regime was not studied in [8]. In fact, it was claimed in [8] that the HIC cannot be used for UHF MRI (operating frequency 298 MHZ). In work [16], the authors designed a similar coil operating in the transmission regime in the range of 300 MHz and used it for scanning knee and hand in a UHF MRI setup. The main difference compared to [8] (besides of evidently different geometric parameters) was a capacitor connected to the antenna in parallel to the receiver instead of a parallel inductor used for the antenna matching in the initial work [8]. In [16], authors used a HIC matched as in [8] for receiving the echo-signal and the same HIC with different matching circuit (using different capacitors) for transmitting the primary signal. However, the necessity for using different matching networks for transmit and receive was not explained. Also the authors do not compare their transmitting HIC compared to a conventional coil used in a UHF MRI (see e.g. in [8]).

In the next section, we discuss the underlying physics of a HIC in both transmission and reception regimes. We prove that in the transmission mode the HICs introduced in [8], [16] have no advantages compared to conventional coils. Further, we show that even in the receiving regime a low-impedance reverse pre-amplifier is needed to suppress the current in the coil. Finally, using the perturbation approach we design a modified HIC operating in the transceiver regime. Our numerical results prove the applicability of the designed HIC for MRI scanning. We prove numerically and experimentally that the suggested HIC is advantageous compared to a conventional transceiver coil.

II. THEORY OF HIC

A. TRANSMIT REGIME

A schematic view of HIC introduced in [8] and [16] is shown in Fig. 1. Due to the size of the coil and the resonance frequency ($r_0 = 40$ mm and 123 MHz in [8] used for 3 T MRI), the current distribution over the outer part of the shield is uniform [17]. In accordance to the theory of loop antennas, only the magnetic mode is present. As to the input impedance, it can be found from the circuit model. In this model, the antenna represents two transmission lines formed by the inner wire and the inner side of the shield connected via the load formed by the outer side of the shield. Both coaxial

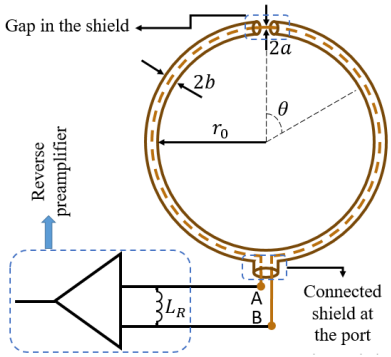

FIGURE 1. Schematics of a HIC suggested in [8].

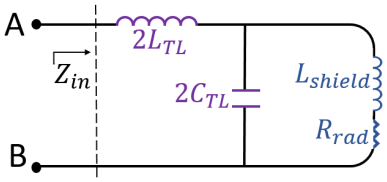

FIGURE 2. Circuit model of a HIC from work [8] in the transmission mode.

lines are connected to this external loop by the cut in the shield. The corresponding circuit model shown in Fig. 2 was, in fact, suggested long ago in [17]. Here L_{TL} and C_{TL} are, respectively, inductance per unit length and capacitance per unit length of the coaxial cable multiplied by πr_0. R_{rad} is radiation resistance and L_{shield} is the inductance both referring to the outer surface of the cable loop. The radiation resistance of a circular loop of radius $r_0 + b$ is calculated as that of a loop magnetic dipole [8] and the inductance is as follows [17]:

$$L_{shield} \approx \mu r_0 (ln\frac{8r_0}{b} - 2) \tag{1}$$

With this model, we calculated the resonance frequency very close to that found in [16] from a different model. At the resonance frequency, the input impedance is real and its value drastically exceeds R_{rad}. Therefore, in order to radiate the needed signal power, we need a very high input voltage of the coil [16]. Thus, the transmitting HIC acts as a conventional loop antenna loaded by a capacitor on top (as it was correctly noticed in [17]). However, though the input impedance at the resonance is high compared to R_{rad}, the coupling coefficient is the same and the electromotive force induced by an adjacent HIC is comparable with the voltage feeding the reference HIC. To decouple the neighbouring HICs, one still needs to overlap them as if they were usual loop antennas. Our simulations show that the coupling between transmitting HICs in a planar array is higher than that in a similar array of usual capacitively loaded loops of the same size. Fig. 3 shows the simulated S-parameters for two HICs and for two usual loop antennas resonating at the same frequency when the distance between the edges of the loops is the same ($\lambda/33$) and the overall sizes of the loops are the same (there is no phantom beneath the coils in this simulation). We see that S_{12} for the pair of HICs is equal to -1.13 dB at the resonance and for the

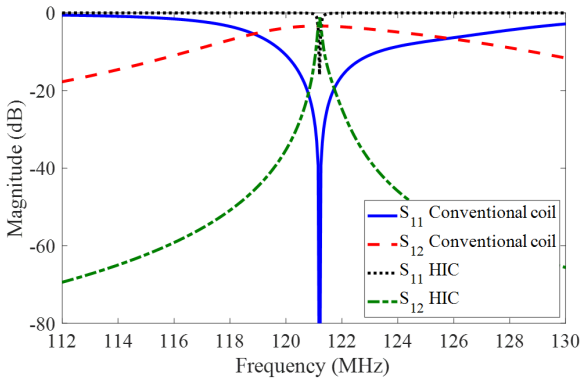

FIGURE 3. S-parameters of two closely (the gap equals $\lambda/33$) located conventional loops and those of two closely located HICs in free space.

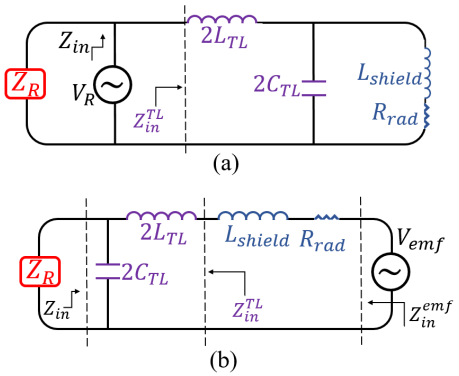

FIGURE 4. (a) Conventional circuit model of a receiving HIC (the same as in the transmission mode). (b) Proposed circuit model of the HIC in the receiving regime.

pair of conventional coils it is lower – $S_{12} = -3.36$ dB. This is not surprising – we have already noticed that in the loops with capacitive loads the electric coupling and the magnetic coupling nearly cancel out. We have also simulated a structure in which two transmitting HICs (and two conventional loops for comparison) overlap such that mutual inductance is nullified. Overlapping these HICs we have decreased the mutual coupling to the same level as for overlapping loops. Moreover, our simulations have shown that in presence of the human body phantom, the input impedance of the HICs manifests a higher sensitivity to the phantom parameters (for example, input impedances of the HIC in the presence of a 50 mm distanced phantom with permittivity $\epsilon_r = 46$ and $\epsilon_r = 80$ are respectively 27650 and 21200 ohm; while the input impedance of the conventional coil in the same situation differs from 0.9 to 1.2 ohm. Needless to say that by changing phantom parameters, resonance frequency of the coil shifts). Thus, matching of these HICs will be in practice more difficult then conventional coils.

B. RECEIVE REGIME

As we have seen, the antenna suggested in [8] was, first, introduced in work [17], where its correct model for the transmission regime was presented. As to the receiving regime, the potential for better decoupling in the antenna array compared to conventional loops was mentioned in [17]. However, the receiving regime of the HIC was not explained. Here we present an alternative model for HIC in reception mode. We will discuss the deviations from the conventional way of understanding HICs and will demonstrate that the model correctly predicts the conditions under which better decoupling can be achieved.

In the conventional model, the input impedance in the receiving regime is defined in the same place as in the transmission regime. The electromotive force (EMF) V_{emf} induced in the antenna is recalculated to the effective voltage V_R applied to the receiver in the same place. In both transmission and reception regimes, all circuit parameters of the antenna are the same. Therefore, the equivalent circuit seems to be that shown in Fig. 4(a), where Z_R is the output impedance of the receiver. In this model, the small inductance $2L_{TL}$ acts nearly as a short-circuit connector, and the capacitance $2C_{TL}$ forms a parallel circuit with the inductance L_{shield}. Since the input resistance of a parallel circuit at the resonance is very large. Since the voltage V_R is finite and $Z_{in} \rightarrow \infty$ (input resistance of the parallel circuit by $2C_{TL}$ and L_{shield} is very high at the resonance frequency) the current flowing at the antenna input is negligibly small. Thus, the receiver with impedance Z_R is excited by an ideal voltage source V_R which is almost decoupled with the external loop. The receiver is driven solely by an induced voltage, induced currents are not involved. Therefore, two receivers connected to two HICs in an array should be decoupled [8]. However, we find that this is not the correct decoupling mechanism for HICs.

In fact, the mutual coupling is not determined by the current flowing at the antenna input and therefore its small magnitude is not relevant. The effective antenna current responsible for the coupling flows at the same place where the induced EMF is formed. For a HIC V_{emf} is referred to the antenna top where the receiving (and scattering) loop formed by the cable exterior is connected to two halves of the cable loop mutually connected on the bottom through the load Z_R. Thus, V_{emf} is connected through L_{shield} (responsible for V_{emf}) and R_{rad} (responsible for scattering) to the input impedance Z_{in}^{TL} of a loaded transmission line. Since two semicircles of cable are connected by Z_R, this Z_{in}^{TL} is different from that shown in Fig. 4(a). Fig. 4(b) depicts the proposed circuit model in the receiving regime, where we clearly distinguish the impedance Z_{in} seen by the receiver and the impedances seen by the induced voltage. Adding an inductance L_R as it was done in [8] and shown in Fig. 1, we engineer a parallel circuit formed by $2C_{TL}$ and L_R. Since the resonant load of the transmission line to which the source is connected becomes large at the operation frequency, the relevant antenna current becomes small. A preamplifier with high output, also shown in Fig. 1 (note that its necessity was mentioned in [17] without any explanation) ensures that the moderate output impedance of the receiver does not shunt the parallel circuit seen by the antenna current. In our model, the input impedance for the induced voltage is as follows:

$$Z_{in}^{emf} = Z_{in}^{TL} + Z_L^{shield} + R_{rad} \tag{2}$$

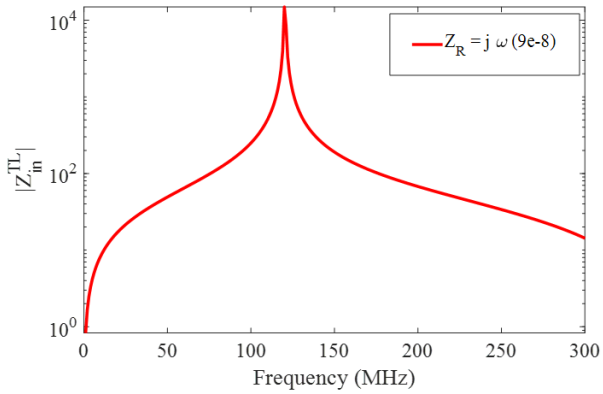

FIGURE 5. Input impedance of the transmission line depicted in Fig. 4(b) versus frequency (log scale). Design parameters of a HIC are taken from [8].

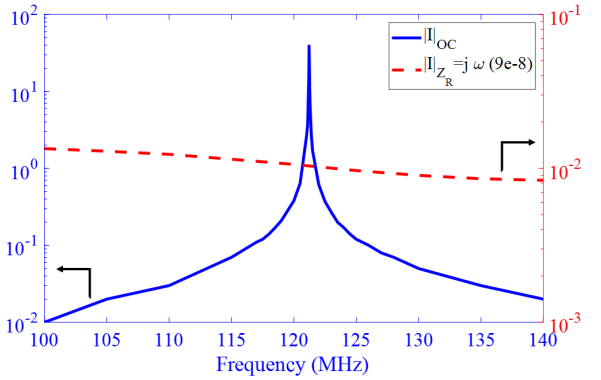

FIGURE 6. Induced current over the HIC with different loadings, when the port AB is open – blue line – and when the port AB is connected to a 90 nH inductor –red line.

where

$$Z_{in}^{TL} = Z_0 \frac{Z_R + jZ_0 tan(\beta l)}{Z_0 + jZ_R tan(\beta l)}. \tag{3}$$

Here Z_0 is characteristic impedance of the cable, $l = 2\pi r_0$ is the total length of the cable and $\beta \approx \omega/c$ is propagation constant in it. As to Z_R, it is a parallel connection of L_R and the pre-amplifier input impedance. The antenna input impedance seen by the receiver is calculated as follows:

$$Z_{in}{}^{-1} = 2j\omega C_{TL} + \frac{1}{R_{rad} + j\omega(L_{shield} + 2L_{TL})}. \tag{4}$$

If Z_R is very small, it shorts the capacitance $2C_{TL}$, the induced voltage is loaded by a small inductance $L_{shield}+2L_{TL}$, the current flowing through V_{emf} is large and the HICs in the array are strongly coupled. If Z_R is very large, the induced voltage is loaded by a series circuit with inductance $L_{shield} + 2L_{TL}$ and capacitance $2C_{TL}$. This circuit resonates exactly at the same frequency where Z_{in} experiences the parallel resonance i.e. at the operation frequency of the HIC. Then the current flowing through V_{emf} is large again. Both these regimes do not result in decoupling. Meanwhile, if $Z_R = j\omega L_R$ and L_R is properly chosen, the induced voltage in a HIC sees a parallel resonance at the operation frequency of the antenna, and such HICs in an array are really decoupled as in [8].

In Fig. 5 we present Z_{in}^{TL} corresponding to Fig. 4(b) for $Z_R = j\omega(9e-8)$. In these calculations, we used Eqs. (2) and (3) instead of a simplistic model with lumped elements as depicted in Fig. 4(b). The design parameters of the HIC and the value $L_R = 90$ nH were taken from [8] where this inductance was connected in parallel to a pre-amplifier with megaohm input. We see that the inductive matching grants not only huge resonant values to $|Z_{in}^{TL}|$ but also large values beyond the resonance (compare to radiation resistance of the HIC). Therefore, the decoupling functionality of a HIC in the receiving regime is broadband. In fact, for a conventional coil, the input impedance seems by V_{emf} almost equals to radiation resistance near the resonance frequency which is in range of couple of ohms (huge induced current over the coil); while for the HIC the input impedance is more than hundreds of ohm (very high compared to radiation resistance) from 70 MHz to 170 MHz which results in a very small induced current over the HIC. Thus, our model is in line with unexplained claims of [17] and with practical results of [8].

For better validation, the current induced on the exterior of a receiving HIC shied has been calculated in computer simulation technology (CST) Microwave Studio. The source was a plane wave with a magnetic field orthogonal to the HIC plane. The current has been calculated for two values of L_R: $L_R \to \infty$ (open-circuit case) and $L_R = 90$ nH that as we have seen grants the parallel resonance at the antenna operation frequency for both antenna input and output. The result is presented in Fig. 6. It confirms what we have claimed above: when the port is open, the induced voltage is really connected to a series circuit and this harmful resonance occurs at the antenna operation frequency. Then the induced current increases drastically i.e. in an array our HICs will be coupled strongly. When the port impedance is inductive and this inductance is sufficiently large, the harmful series resonance for the induced current does not occur and the current keeps small in the range $70 - 170$ MHz. Now, it is pretty clear why the HICs were decoupled in a receiving array [8], why the decoupling of the transmitting HICs required two different capacitors for transmission and reception regimes (transmission and reception regimes have different circuit models), and why it was not better than that in an array of capacitively loaded loops.

III. DESIGNING TRANSCEIVER HIC

The previous insights serve as an introduction to the main purpose of this paper – design of a transceiver HIC for scanning the human head in 7 Tesla MRI with 8 channel pre-amplifier. It means that the radius of the HIC should be larger than the HICs of [8], [16] where either the frequency range was lower or the scanning area was limited to the hand or the knee. For our purpose, the radius of a transceiver HIC should be $r_0 = 80$ mm to cover the whole head with 8 coils. In this case, the perimeter of the coil is $P_{HIC} = 2\pi r_0 \approx \lambda/2$ which means that the HICs of works [8], [16] cannot be considered as electromagnetically small in the range of 300 MHz.

In these HICs, high-order multipoles will be induced at such frequencies. This effect will make an analytical model and the design procedure very difficult. A transceiver HIC should be designed in such a way that only two fundamental modes of the coil – magnetic dipole and electric dipole – would exist at the operation frequency. Moreover, it should be obtained in the situation when the electromagnetic size of the coils is larger than in works [8], [16]. So, we have to raise the fundamental resonance of a coil from 123 MHz to nearly 300 MHz with a simultaneous increase of the HIC size. Next, we have to reduce $|S_{12}|$ for two neighboring HICs in the transmission regime.

We have solved the second problem almost in the same way as discussed above. It is possible to engineer a Huygens regime in a HIC obtaining an electric dipole mode due to a capacitive load of the external loop. It implies additional cuts of the shield. If the optimal position of the cut is not the loop bottom (a feeding point), we should not make one cut aside the loop. Otherwise, we will make our HIC bianisotropic, bring quadrupole components in the loop current and strongly complicate our task. Thus, we should make two symmetrically located cuts in the shield. Next, according to the perturbation approach (see e.g. in [19]), we add a perturbation at the points where the induced current component corresponding to the magneto-dipole mode is high enough. This perturbation should result in the raise of the resonance frequency for the magnetic mode. This perturbation can be a simple cut of the inner wire. These two cuts (also symmetrically located) do not break the current because two broken ends will be coupled via the interior side of the shield. Depending on the position where we add these cuts (near the maxima of the charge distribution or near the maxima of the current distribution), these cuts can be modeled as loading elements – either inductors or capacitors. The exact position of these gaps should be found numerically. Fig. 7(a) shows the new HIC with cuts of the inner wire (angles α) and the shield (angles β). These angles should be chosen such that our large HIC resonates at 298 MHz (Larmor frequency of hydrogen at 7T) with balanced electric and magnetic current modes. More details are provided in the next section.

For this properly designed HIC, we show in Fig. 7(b) both near-zone magnetic field distribution in the loop plane and current distribution over the external loop. If two such HICs are positioned back to back (upside down), they do not produce magnetic flux over each other and are decoupled not only in the reception regime but also in the transmission regime. However, as well as for the conventional loops this arrangement cannot be extended to arrays with more than two coils. In this case we may arrange the chain of HICs with alternating locations of the antenna inputs (see Fig. 7(c)). Then the closest coils will be weakly coupled because in Fig. 7(b) we see that the near field aside the loop is quite weak. Below we will see that this solution grants a reduction of the coupling in the array with respect to the known analogues.

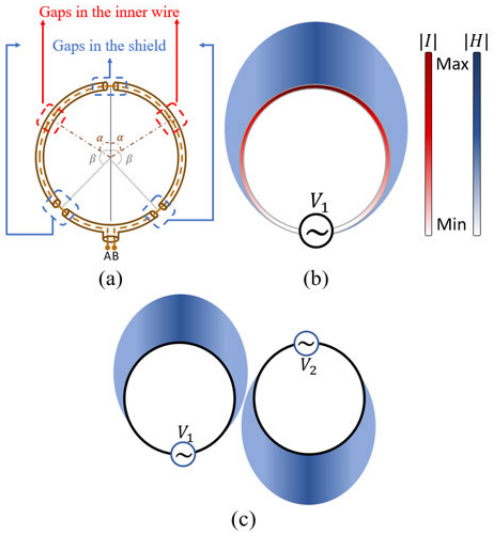

FIGURE 7. (a) Schematic view of the new coil with added gaps in positions α and β. (b) Current distribution over the external loop and radiated magnetic field in the near zone (both magnetic and electric dipoles are balanced at the operation frequency 298 MHz). (c) Alternative arrangement of the HICs to minimize coupling.

Notice that in the receiving regime the performance of our coil is quite similar to that of a HIC from [8]. Of course the non-uniformity of the induced current in the case of three gaps in the cable shield influences the near field coupling coefficients. However, the main factor of decoupling stays the same – the high impedance seen by the induced voltage.

IV. NUMERICAL VERIFICATION

We simulated the performance of our HIC using CST Microwave Studio, in both Frequency and Time Domain solvers. In Time Domain solver, a lumped voltage source with 50 ohm reference impedance is connected to the antenna port. The average number of cells used in our simulations by this solver was $\sim$ 980000. To find out resonance frequency of the HIC using this lumped source, one has to check the impedance matrix and recalculate s-parameters based on impedance matrix. In Frequency Domain solver, a lumped power source with 50 ohm reference impedance is connected to the antenna port. The average number of cells in these simulations was $\sim$ 230000 with the minimum 15 meshes around the corners. using this type of lumped port, one is able to calculate s-parameters directly. To verify the applicability of the perturbation method to our HIC, we simulated the transceiver HIC with different positions of the added perturbing gaps. In the simulation, $r_0 = 80$ mm, $b = 1.2$ mm, $a = 0.5$ mm and the dielectric permittivity of the coaxial cable is $\epsilon_r = 2.2$. Similar to the HIC presented in [8], there is a gap on top of our transceiver HIC to make the coil radiative. To raise the resonance frequency we added two symmetrically positioned cuts to the shield and varied the angle β shown in Fig.7(a) from 20° to 160°. The resonance frequency of the coil changes as depicted in Fig. 8 – there is no local maximum on the red line because the maximum corresponds to $\beta = 180°$. Next, we fixed the optimal $\beta = 180°$ and added

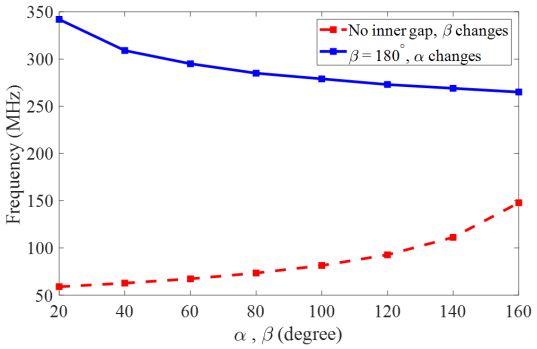

FIGURE 8. Resonance frequency of the modified HIC with respect to the two symmetrically added gaps to the shield – red line – and with respect to the two symmetrically added gaps to the inner wire while there is one gap at $\beta = 180°$ on the shield – blue line.

two more symmetrically positioned cuts to the inner wire at the angle α, changing it also 20° to 160°. The result is a blue line in Fig. 8. Again, when these added gaps in the inner wire are closer to the top, where also the electric field produced by the electric dipole mode is maximal, the resonance frequency increases rapidly. When the cuts in the inner wire are close to those in the shield, their impact is low because they start to operate as a single perturbing element.

Thus, introducing our additional cuts we may increase the resonance frequency of our enlarged HIC from 56 MHz up to nearly 350 MHz. Now, let us optimize the angles α and β to create a resonance at 298 MHz and minimize the mutual coupling in an array. In this regime, the electric and magnetic modes of the current are balanced. We simulated two in-plane HICs separated by a 3 cm gap ($\lambda/33$) with antenna inputs located upside down and loaded by L_R in both transmission and reception regimes. In these simulations we found $\beta = 180°$ and $\alpha = 32°$ which grant the required operation frequency and the decoupling in the transmission regime. For two transmitting HICs, we got at 298 MHz $S_{12} = -4.6$ dB; and for two the same size conventional coils located upside down with the same distance from each other when the current distribution over these conventional coils is similar to those of HICs we got $S_{12} = -5.4$ dB. As expected, this value is lower than that obtained for two HICs from [8] – $S_{12} = -1.13$ dB – and obtained for two conventional coils – $S_{12} = -3.36$ dB. In fact, presence of electric dipole mode reduces the coupling when these coils are located upside down next to each other. Although coupling between our transceiver HICs is not lower than that of the conventional coils, due to added gaps bandwidth of our HICs is wide and the performance of the HICs will be more stable compare to conventional coils with respect to different loading. Overlapping our transceiver HICs helps to further reduce the coupling. Note that in the presence of a body phantom with high permittivity the coupling between the antennas in the array is further reduced. In this case, the lower coupling granted by our HICs compared to conventional coils, makes the S-parameters more stable in the presence of a phantom with varying sizes and permittivity.

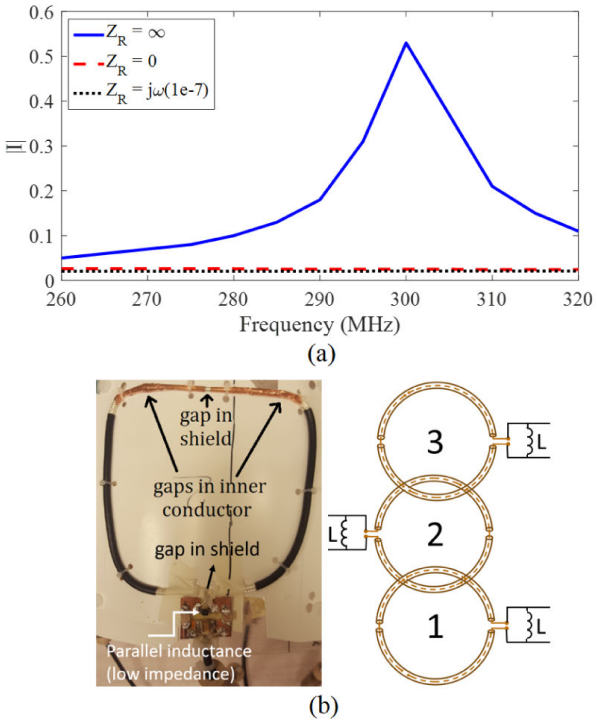

FIGURE 9. (a) Simulation of the mean induced current in the receiving regime for three different loads at the port. (b) Fabricated transceiver HIC (with the matching circuit) and the arrangement of the ports in the array (inset).

In the reception regime, using the optimal $L_R = 100$ nH, we obtained an S_{12}-parameter for our HICs nearly equivalent to two HICs introduced in [8]. We have also checked that for the open receiving port the induced current at the resonance becomes large and non-uniform. Fig. 9(a) shows the simulation result for the induced current for three values of Z_R. Since the induced current is not uniform over the external loop, the current in this plot is the mean value (averaged over the loop perimeter). This result confirms once more what we have claimed about the decoupling in the reception regime.

V. MRI APPLICABILITY

To check the applicability of our HIC to MRI application, we numerically studied performance of the transceiver HIC regarding MRI criteria. For this study, we simulated two cases: (1) our HIC is located at the distance 50 mm over a cubic phantom with dimensions $250 \times 250 \times 250$ mm^3, $\epsilon_r = 46$ and $\sigma = 0.5\ S/m$; (2) a conventional loop with the same size of our HIC located at the same place. The values for the phantom permittivity and conductivity are selected in a way to imitate human head features. For both of these cases a lumped power source with internal impedance 50 ohm is connected to the coils feeding port without any matching circuit. Moreover, to have almost the same current distribution over the conventional coil and our HIC, three capacitors ranging from 1 to 2.5 pF are employed in the conventional loop. Fig.10(a) shows schematic view of these simulated structures. The criteria need to be studied for MRI application are as follow:

- transmit efficiency: how well is the power used.

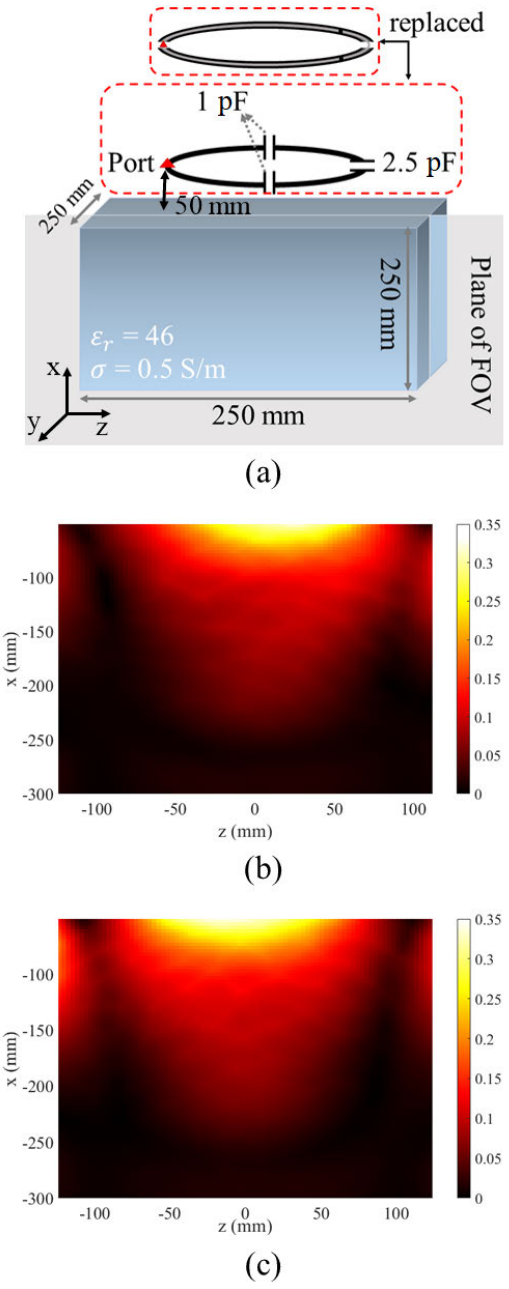

FIGURE 10. (a) Structures in the simulations (once with conventional loop and once with the HIC). (b) The HIC field of view, (c) the conventional loop field of view.

- Specific absorption rate (SAR) efficiency: how much $B_1{}^+$ can be achieved within a human body without doing harm.
- Signal to noise ratio (SNR): how well the signal is receive from the phantom.
- Filed of view (FOV): distribution of $B_1{}^+$ in the phantom.
- Operational bandwidth (BW): at least 500 KHz is required for the application.

In these simulations the power source applies 0.5 W over a wide range of frequencies. Depending on the input impedance of the coils in the transmission regime, part of the power is accepted (P_{acc}) and the rest is reflected back to the source. In cases (1) and (2) the accepted power is 0.01 W and 0.42 W respectively. Due to very high input impedance of the HIC, it was expected that most of power will be reflected to the power source. The accepted power is radiated in the surrounding media as electromagnetic power and mostly absorbed in the phantom. The absorbed power ($P_{absorbed}$) in the phantom for cases (1) and (2) is 0.009 W and 0.38 W. The relationship for calculating transmit efficiency is as follows:

$$Transmit_{eff} = B_1{}^+/\sqrt{P_{acc}} \tag{5}$$

where $B_1{}^+ = 0.5(B_x + jB_y)$. To calculate transmit efficiency, first we calculated B_x and B_y at every points in the phantom, then we calculated $|B_1{}^+|$ at these points and took the mean of it. The transmit efficiency for cases (1) and (2) is 0.071 and 0.072 respectively. The relationship for calculating SAR efficiency is:

$$SAR_{eff} = B_1{}^+/\sqrt{SAR_{max}} \tag{6}$$

where $SAR_{max} = \sigma |E|_{max}{}^2/\rho$ and $\rho = 997$ kg/m^3 is density of the phantom. Obtained SAR_{eff} for cases (1) and (2) is 0.054 and 0.053 respectively. The next criterion is SNR which calculated as follows:

$$SNR = B_1{}^-/\sqrt{P_{absorbed}} \tag{7}$$

where $B_1{}^- = 0.5(B_x - jB_y)$. $P_{absorbed}$ contains all losses such as phantom losses, radiation losses and losses in the coil; and as a result, its value is the same as P_{acc}. Accordingly, SNRs for these cases are the same and equal to 0.074. Moreover, FOV for these cases are shown in Fig.10(b) and (c). In these figures, $|B_1{}^+|$ is depicted on the plane $y = 0$ (the plane is shown in Fig.10(a)). Due to non-uniform current distribution over the HIC and the conventional coil, $|B_1{}^+|$ is not symmetric with respect to z axis. For the HIC, the current is maximum at the position opposite to the feeding point while for the conventional coil the current is maximum at the feeding point (because of non-uniformly distributed capacitors). Other aspects are almost similar in these FOVs. Finally to calculate BW of our HIC we added a matching circuit consisting of a parallel inductor and a series capacitor between the HIC and the power source (the inductor is connected to the HIC feeding point). In this situation, the HIC is well matched $|S_{11}| = -75$ dB and BW is 5.7 MHz (1.9% relative bandwidth). Considering required BW for MRI scanning $\sim$ 500 KHz, the obtained bandwidth is more than enough. With respect to these criteria, we conclude that the performance of our HIC is as good as the conventional coil while coupling between our HICs is smaller compared to conventional ones in both transmit and reception regimes.

VI. EXPERIMENTAL VERIFICATION

To verify the performance of our HICs experimentally, we fabricated an array of 3 transceiver HICs operating at 298 MHz and arranged as is shown in Fig. 9(b). Dimensions of our HICs were the same as those we have found above via simulations though the circular shape of the loops was slightly modified when we fixed them in the array. Fig. 9(b) shows one fabricated transceiver HIC with its matching circuit.

The HICs were fabricated using coaxial cable type Huber Suhner, RG 223U in UMC Utrecht lab. In the matching circuit, the inductance $L_R = 170$ nH was connected in parallel with a capacitance. This matching circuit allowed us to combine the proper Z_R in the receiving regime together with the matching in the required operation band. The preamplifiers were embedded in the 7 T Philips MRI machine. Due to lower coupling between two transceiver HICs compared to conventional coils, we could match our HICs easier and the S-parameters are more stable when we vary the parameters of the phantom. Here, it is worth to note that overlapping the loops decouples the adjacent ones quite well, but the coupling between non-adjacent loops makes the S-parameters of these loops sensitive to the ambient. A slight variation of the phantom size, permittivity or conductivity causes a deviation in the resonant S-parameters and the decoupling of adjacent loops worsens.

Our HICs, by creating weaker fields aside, should grant lower coupling for non-neighboring elements and the array should be more stable with respect to the ambient. To verify this, we measured S-parameters of an array constituted of three transmitting HICs in the presence of three different cylindrical phantoms and compared the results with those for an array of three conventional capacitively loaded coils. The phantoms were as follows: (1) salty water with $\epsilon_r = 75$, conductivity $\sigma = 0.5$, length 200 mm and radius 75 mm (strong loading in MRI terminology), (2) salty water with reduced radius 50 mm (spherical shape), other parameters are same (moderate loading), (3) vegetable oil with $\epsilon_r = 3$, conductivity $\sigma = 0.01$, length 250 mm and radius 60 mm (weak loading). The conventional coils were made of insulated copper wires with 3 mm core diameter. These loop coils had a radius $r_0 = 80$ mm and six inserted capacitors, American Tech Ceramics 100E series, ranging from 2.7 to 3.3 pF making the loop resonant at the same frequency (298 MHz). The conventional array was optimized for the case of strong loading. In the measurement, to be more realistic, we put the array of three HICs over a transparent plastic cylindrical shell with length 250 mm and radius 170 mm and located the phantoms in its center. Then we put the structure in to a dummy bore – a big metallic cylinder – which imitates MRI machine effects over the antennas performance. Fig. 11 shows the structure in the dummy bore. Notice that the matching circuits were chosen based on this configuration. Then s-parameters of the antennas have been calculated using Vector Network Analyzer.

Fig. 12 shows S-parameters of both arrays in the presence of three different loads. As we expected, both S_{ii} and S_{ij} of the transceiver HIC array are more stable compared to the conventional coil array. Our HIC provides better decoupling for non-adjacent coils 1 and 3. While changing the phantom load, S_{12} keeps stable (-15 dB) for HICs whereas for the loop array we have $S_{12} = -15$ dB only for the strong loading. For the moderate and weak loadings the coupling increases to $S_{12} = -12$ dB and $S_{12} = -10$ dB, respectively. Our numerical and experimental results clearly show that the

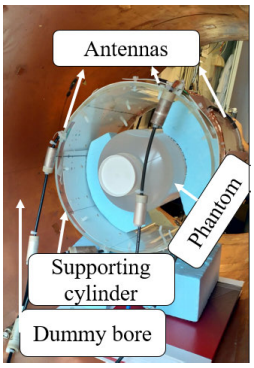

FIGURE 11. Structure including antennas and phantom in the dummy bore.

		Strong loading			Moderate loading			Weak loading		
	Channel	1	2	3	1	2	3	1	2	3
HIC	1	-32	-15	-21	-22	-15	-18	-20	-15	-18
	2	-15	-20	-20	-15	-17	-22	-15	-16	-22
	3	-21	-20	-18	-18	-22	-15	-18	-22	-14
Usual coil	1	-15	-15	-12	-15	-12	-11	-12	-10	-12
	2	-15	-24	-23	-12	-18	-15	-10	-12	-16
	3	-12	-23	-10	-11	-15	-8	-12	-16	-5

FIGURE 12. Measurement results (in dB) for resonant S-parameters of the antenna array of three HICs and the same for three conventional coils in presence of three different phantoms.

suggested transceiver HIC is advantageous with respect to the conventional coils and preserves the advantages of the receiving HIC from [8] in the transmission regime.

VII. CONCLUSION

In this paper, the physics of the previously introduced high-impedance coils for MRI was comprehensively studied in both transmission and reception regimes. We have found that in the transmission regime these HICs are not advantageous. We introduced an adapted transceiver HIC which is truly beneficial with respect to conventional coils at 300 MHz. We have proven it analytically using the equivalent circuit and numerically, using CST simulations. The performance of the adapted HIC for MRI application was numerically studied. To confirm our theory experimentally we fabricated an array of transceiver HICs and an array of conventional loops for comparison. The coupling in the transmitting regime is indeed lower for our HICs and our array is more stable to variations in the phantom load. The stability refers to both matching and decoupling.

REFERENCES

[1] W. Mao, M. B. Smith, and C. M. Collins, "Exploring the limits of RF shimming for high-field MRI of the human head," *Magn. Reson. Med.*, vol. 56, no. 4, pp. 918–922, Oct. 2006.

[2] T. S. Ibrahim and L. Tang, "Insight into RF power requirements and B_1 field homogeneity for human MRI via rigorous FDTD approach," *J. Magn. Reson. Imag.*, vol. 25, no. 6, pp. 1235–1247, Jun. 2007.

[3] N. I. Avdievich, J. W. Pan, and H. P. Hetherington, "Resonant inductive decoupling (RID) for transceiver arrays to compensate for both reactive and resistive components of the mutual impedance," *NMR Biomed.*, vol. 26, no. 11, pp. 1547–1554, Nov. 2013.

[4] M. S. M. Mollaei, A. Hurshkainen, S. Kurdjumov, S. Glybovski, and C. Simovski, "Passive electromagnetic decoupling in an active metasurface of dipoles," *Photon. Nanostruct.-Fundamentals Appl.*, vol. 32, pp. 53–61, Dec. 2018.

[5] A. A. Hurshkainen, T. A. Derzhavskaya, S. B. Glybovski, I. J. Voogt, I. V. Melchakova, C. A. T. van den Berg, and A. J. E. Raaijmakers, "Element decoupling of 7 T dipole body arrays by EBG metasurface structures: Experimental verification," *J. Magn. Reson.*, vol. 269, pp. 87–96, Aug. 2016.
[6] P. B. Roemer, W. A. Edelstein, C. E. Hayes, S. P. Souza, and O. M. Mueller, "The NMR phased array," *Magn. Reson. Med.*, vol. 16, no. 2, pp. 192–225, Nov. 1990.
[7] X. Yan, J. C. Gore, and W. A. Grissom, "Self-decoupled radiofrequency coils for magnetic resonance imaging," *Nature Commun.*, vol. 9, no. 1, p. 3481, Dec. 2018.
[8] B. Zhang, D. K. Sodickson, and M. A. Cloos, "A high-impedance detector-array glove for magnetic resonance imaging of the hand," *Nature Biomed. Eng.*, vol. 2, no. 8, pp. 570–577, May 2018.
[9] A. Kurs, A. Karalis, R. Moffatt, J. D. Joannopoulos, P. Fisher, and M. Soljacic, "Wireless power transfer via strongly coupled magnetic resonances," *Science*, vol. 317, no. 5834, pp. 83–86, Jul. 2007.
[10] B. Tierney and A. Grbic, "Planar shielded-loop resonators for wireless non-radiative power transfer," in *Proc. IEEE Antennas Propag. Soc. Int. Symp. (APSURSI)*, Jul. 2013, pp. 842–843.
[11] E. Laistler and E. Moser, "Handy magnetic resonance coils," *Nature Biomed. Eng.*, vol. 2, no. 8, pp. 557–558, Aug. 2018.
[12] R. Frass-Kriegl, E. Laistler, S. Hosseinnezhadian, A. I. Schmid, E. Moser, M. Poirier-Quinot, L. Darrasse, and J.-C. Ginefri, "Multi-turn multi-gap transmission line resonators—Concept, design and first implementation at 4.7 T and 7 T," *J. Magn. Reson.*, vol. 273, pp. 65–72, Dec. 2016.
[13] L. Nohava, R. Czerny, M. Obermann, M. Pichler, R. Frass-Kriegl, J. Felblinger, J. C. Ginefri, and E. Laistler, "Flexible multi-turn multi-gap coaxial RF coils (MTMG-CCs): Design concept and bench validation," in *Proc. 27th Annu. Meeting Int. Soc. Mag. Res. Med.*, 2019, p. 0565.
[14] R. Czerny, L. Nohava, R. Frass-Kriegl, J. Felblinger, J. C. Ginefri, and E. Laistler, "Flexible multi-turn multi-gap coaxial RF coils: Enabling a large range of coil sizes," in *Proc. 27th Annu. Meeting Int. Soc. Mag. Res. Med.*, 2019, p. 1550.
[15] M. Obermann, L. Nohava, S. Goluch-Roat, M. Pichler, J. Sieg, J. Felblinger, J. C. Ginefri, and E. Laistler, "Ultra-flexible and light-weight 3-channel coaxial transmission line resonator receive-only coil array for 3T," in *Proc. 27th Annu. Meeting Int. Soc. Mag. Res. Med.*, 2019, p. 1558.
[16] T. Ruytenberg, A. Webb, and I. Zivkovic, "Shielded-coaxial-cable coils as receive and transceive array elements for 7T human MRI," *Magn. Reson. Med.*, vol. 83, no. 3, pp. 1135–1146, Mar. 2020.
[17] L. L. Libby, "Special aspects of balanced shielded loops," *Proc. IRE*, vol. 34, no. 9, pp. 641–646, Sep. 1946.
[18] D. K. Cheng, *Field and Wave Electromagnetics*. New York, NY, USA: Addison-Wesley, 1989.
[19] R. F. Harrington, *Time-Harmonic Electromagnetic Fields*. New York, NY, USA: Wiley, 2001, pp. 316–320.

MASOUD SHARIFIAN MAZRAEH MOLLAEI was born in Tehran, Iran, in 1989. He received the B.Sc. degree in electrical engineering from Imam Khomeini International University, Qazvin, Iran, in 2013, the M.Sc. degree in electrical engineering from the Iran University of Science and Technology (IUST), Tehran, in 2016. He is currently pursuing the Ph.D. degree with the Department of Electronics and Nanotechnology, Aalto University, Espoo, Finland. His thesis is to introduce novel method for decoupling dipole and loop antenna arrays for 7 T MRI.

He was developing theoretical and experimental techniques for ultrahigh-field magnetic resonance imaging with Aalto University. His current research interests include array antenna, antenna decoupling, metamaterials, and photonics.

CAREL C. VAN LEEUWEN was born in Amsterdam, The Netherlands, in April 1990. He received the B.Sc. degree in physics and astronomy and the master's degree in biomedical imaging science from Utrecht University. He is currently pursuing the Ph.D. degree with the Department of Radiology, UMC Utrecht, The Netherlands. His current research interests include electromagnetic modeling and RF engineering for high-filed MRI.

ALEXANDER J. E. RAAIJMAKERS received the M.Sc. degree in applied physics from the University of Groningen, in 2004, and the Ph.D. degree (research project) from the Radiotherapy Department, University Medical Center Utrecht. His project involved the investigation of radiotherapy dose distributions with the presence of magnetic field for (hypothetical) MRI-guided radiotherapy. He has discovered the Electron Return Effect (ERE). From 2008 to 2010, he received the Casimir Grant on the Development of New RF Transmit and Receive Coils for High-Field MRI, for which he was in part stationed with Philips Medical Systems, Best, The Netherlands. He has acquired extensive knowledge on EM physics with MRI and RF Engineering. Since 2013, he has been an Assistant Professor with the 7T Research Group, Department of Radiology, UMC Utrecht. In 2016, he was an Assistant Professor with the Research Group Medical Image Analysis, Eindhoven University of Technology. His research interest includes newly installed seven-tesla MRI scanner.

CONSTANTIN R. SIMOVSKI was born in Leningrad, Russia, in December 1957. He received the Diploma degree in radio engineering (engineer researcher), the Ph.D. degree in electromagnetic theory, and the Doctor of Sciences degree from St. Petersburg State Polytechnic University (Leningrad Polytechnic Institute and State Technical University), St. Petersburg, in 1980, 1986, and 2000, respectively.

From 1980 to 1992, he was with the Soviet Scientific and Industrial firm Impulse. In 1986, he defended the Candidate of Science (Ph.D.) thesis (study of the scattering of Earth waves in the mountains) with the Leningrad Polytechnic Institute. In 1992, he held an Assistant position with the St. Petersburg University of Information Technologies, Mechanics and Optics, where he was an Assistant Professor, from 1994 to 1995, and from 1995 to 2001, he was an Associate Professor. Since 1999, he has been involved in the theory and applications of 2-D and 3-D electromagnetic band-gap structures for microwave and ultrashortwave antennas. In 2000, he defended the thesis of Doctor of Sciences (a theory of 2-D and 3-D bianisotropic scattering arrays). Since 2012, he has been a Full Professor with the Department of Electronics and Nanotechnology, Aalto University. His current research interests include metamaterials for microwave and optical applications including optics of metal nanoparticles.